FULL PAPER

Yolk–Shell Hybrid Materials with a Periodic Mesoporous Organosilica Shell: Ideal Nanoreactors for Selective Alcohol Oxidation

Jian Liu, Heng Quan Yang, Freddy Kleitz, Zhi Gang Chen, Tianyu Yang, Ekaterina Strounina, Gao Qing (Max) Lu,* and Shi Zhang Qiao*

This contribution describes the preparation of multifunctional yolk–shell nanoparticles (YSNs) consisting of a core of silica spheres and an outer shell based on periodic mesoporous organosilica (PMO) with perpendicularly aligned mesoporous channels. The new yolk–shell hybrid materials were synthesised through a dual mesophase and vesicle soft templating method. The mesostructure of the shell, the dimension of the hollow space (4~52 nm), and the shell thickness (16~34 nm) could be adjusted by precise tuning of the synthesis parameters, as evidenced by X-ray diffraction (XRD), scanning electron microscopy (SEM), transmission electron microscopy (TEM) and nitrogen sorption investigations. Various metal nanoparticles (e.g., Au, Pt, and Pd) were encapsulated and confined in the void space between the core and the shell using impregnation and reduction of adequate metal precursors. The selective oxidation of various alcohol substrates was then carried out to illustrate the benefits of such an architecture in catalysis. High conversion (~100%) and excellent selectivity (~99%) were obtained over Pd nanoparticles encapsulated in the hybrid PMO yolk–shell structures.

1. Introduction

So-called "yolk–shell" nanostructures or "rattle-type" nanomaterials containing a void space between the core and the outer shell of the material are emerging as an interesting family of complex new hollow nanoarchitectures.[1–4] The enclosed void space of yolk–shell nanoparticles is expected to be useful for chemical storage, compartmentation, and confinement of host–guest interactions. Furthermore, their tunability and functionality in both the core and the inner shell region can endow yolk–shell nanoparticles (YSNs) with new properties, thus rendering them attractive for applications as nanoreactors,[5,6] drug/gene delivery systems,[7,8] surface-enhanced Raman scattering (SERS) technologies,[9,10] and energy storage media.[11–13] Most importantly, the void space in the yolk–shell nanostructure may provide a unique environment for creating concerted actions between the core and a permeable shell. Thus, porous shells with controllable permeability are particularly sought after.

Alongside numerous synthetic methods available to generate hollow nanostructures, several strategies for the preparation of a yolk–shell structure have been developed, including the ship-in-bottle approach,[14] bottom-up or soft templating approaches,[15–18] selective etching approaches,[19–23] template-free approaches,[24,25] Ostwald ripening[26] or galvanic replacement processes,[27] and methods based on the Kirkendall effect.[2] Various yolk–shell colloidal particles and nanoparticles with different chemical compositions, including metal NPs@silica, metal oxide@silica, metal NPs@carbon, metal NPs@metal oxide, metal NPs@polymer, silica@metal oxide, silica@carbon, polymer@polymer, have all been obtained by using the above synthesis methods.[1]

Soft templating approaches have recently been introduced and these are considered as a simple, effective, and general strategy to produce such yolk–shell structures, especially for yolk–shell architectures possessing a permeable porous shell. In particular, YSNs with mesoporous shell can exhibit unique release properties,[7,17] or prevent sintering/aggregation of entrapped catalytic species while promoting diffusion and mass

Dr. J. Liu, T. Y. Yang, Prof. G. Q.(M.) Lu, Prof. S. Z. Qiao
ARC Centre of Excellence for Functional Nanomaterials
Australian Institute for Bioengineering and Nanotechnology
The University of Queensland
QLD 4072, Australia
E-mail: maxlu@uq.edu.au; s.qiao@uq.edu.au
Prof. H. Q. Yang
School of Chemistry and Chemical Engineering
Shanxi University
Taiyuan 030006, P. R. China
Prof. F. Kleitz
Department of Chemistry and Centre de recherche
sur les matériaux avancés (CERMA)
Université Laval
Quebec, G1V 0A6, QC, Canada
Dr. Z. G. Chen
Centre for Microscopy and Microanalysis and School of Engineering
The University of Queensland
QLD 4072, Australia
Dr. E. Strounina
Centre for Advanced Imaging
The University of Queensland
QLD 4072, Australia

FULL PAPER

transfer of reactants,[6] attributes which are very useful in drug/gene delivery and nano-reactor applications.

Although some progress in the synthesis of yolk–shell particles with a nanoporous shell has been achieved, the shells obtained thus far consist essentially of disordered pore structures, with poor level of compositional diversity and functionality. More specifically, the design of yolk–shell particles exhibiting multiple cores with distinct properties, and a functionalised ordered mesoporous shell is still highly desirable in order to develop versatile new nanoreactors and bioactive-molecule delivery systems. Within this context, the integration of both organic and inorganic fragments within the pore walls of periodic mesoporous organosilica (PMO) has been a breakthrough in the area of functional nanoporous materials.[28–31] Since then, a great variety of PMOs exhibiting diverse mesostructures and framework compositions, and controlled particle morphologies (solid spheres,[31] hollow spheres,[32–35] single crystals,[36] helical[37] and core–shell structures[38]) have been described. These hybrid materials have wide perspectives of applications, in areas such as catalysis, selective sorption and separation, biomolecule immobilisation, low *k*-dielectrics, and so forth, owing to the great diversity of available functionalities and their high thermal and chemical stability.[28–31] Therefore, in order to develop optimised nanoreactors and nanocarriers, it could be advantageous to produce YSNs constituted of a well-defined functional PMO shell. This should enable the combination of the benefits of both the yolk–shell architecture and organic–inorganic hybrid PMO functionalities. In addition to this, the use of the void space between the core and the shell in such a system to selectively host some active catalytic species remains to be demonstrated.

With the aim of expending the range of composition and functionality of the yolk–shell nanostructures, we report here for the first time on the construction of multifunctional YSNs consisting of a core of dense silica spheres, a hollow space between core and shell, and an outer PMO-type shell with per-pendicularly aligned mesoporous channels. The new yolk–shell hybrid materials with PMO shell were synthesised through combined mesophase and vesicle dual soft templating method. In particular, we demonstrate that the mesostructure of the shell, the dimension of the hollow space (4~52 nm), and the shell thickness (16~34 nm) can all be well adjusted by precise tuning of the synthesis parameters. Furthermore, the thus-designed multifunctional YSNs possess both large void spaces, enabling proper loading with guest molecules and confine-ment of active metal nanoparticles, and an ordered organic-functionalised mesopore shell allowing for fast diffusion of reactants. The possibility of confining catalytic entities is clearly evidenced by the selective encapsulation in the void space of various metal nanoparticles (e.g., Au, Pt, Pd). To illustrate the benefits of such architecture in catalysis, selective oxidation of various alcohol substrates was then carried out. High conver-sion (~100%) and excellent selectivity (~99%) were obtained
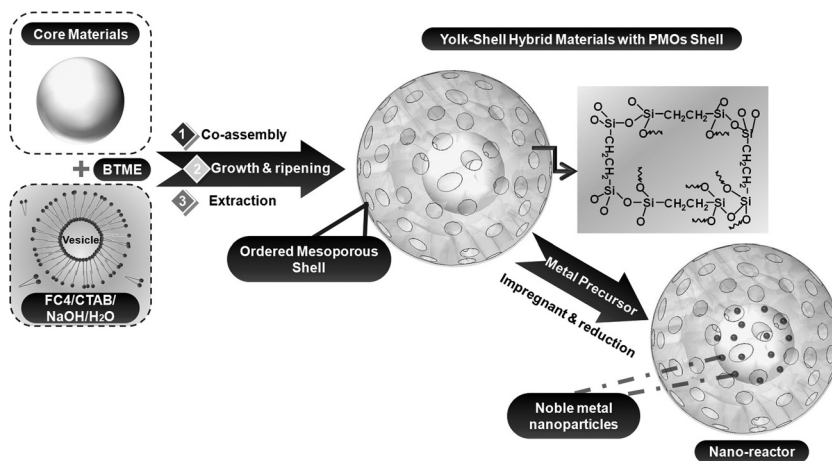
Scheme 1. Synthesis procedure and proposed structure of yolk–shell hybrid materials with a PMO shell.

over Pd nanoparticles embedded in these hybrid PMO yolk–shell structures.

2. Results and Discussion

2.1. Synthesis of Yolk–Shell Hybrid Materials with PMO Shell

The synthesis of the yolk–shell PMO (YS-PMO) hybrid mate-rials is schematically represented in **Scheme 1**. Here, solid silica spheres prepared by the Stober method are selected as an example of core materials. The first step of the material syn-thesis involves the combination of the selected core materials and the vesicles formed in aqueous solution by a fluorocarbon surfactant $[C_3F_7O(CFCF_3CF_2O)_2CFCF_3CONH(CH_2)_3N^+(C_2H_5)_2CH_3I^-]$ (FC4). In the next step, hybrid organosilane-surfactant micellar aggregates, which are built of hydrolysed/oligomer-ised bis(trimethoxysilyl)ethane (BTME) species and cetyltri-methylammonium bromide (CTAB), assemble under basic conditions while surrounding the core-vesicle complex eventu-ally forming an ordered mesostructured organosilica shell via cooperative self-assembly. Under these conditions, the growth of the hybrid organosilica–CTAB mesophase remains confined to the periphery of the vesicle region. Following further growth and ripening process of the shell, induced by condensation of the BTME oligomeric species, a PMO yolk–shell structure can be obtained after removal of both the CTAB and FC4 tem-plates by solvent extraction. The obtained material is denoted as YS-PMO, which consists of a siliceous core, hollow shell, and PMO shell. This dual mesophase and vesicle templating ensures that the organosilica organises around the core vesicle complex to generate the desired yolk–shell nanospheres exhib-iting a PMO shell.

Figure 1 shows representative TEM images of the hybrid yolk–shell material (YS-PMO-1) presenting a 160 nm silica core and a mesoporous shell. The shell thickness is ~20 nm, the hollow void is ~7 nm, resulting in an overall outer diameter of ~220 nm for a single yolk–shell particle (Figures 1a and b).
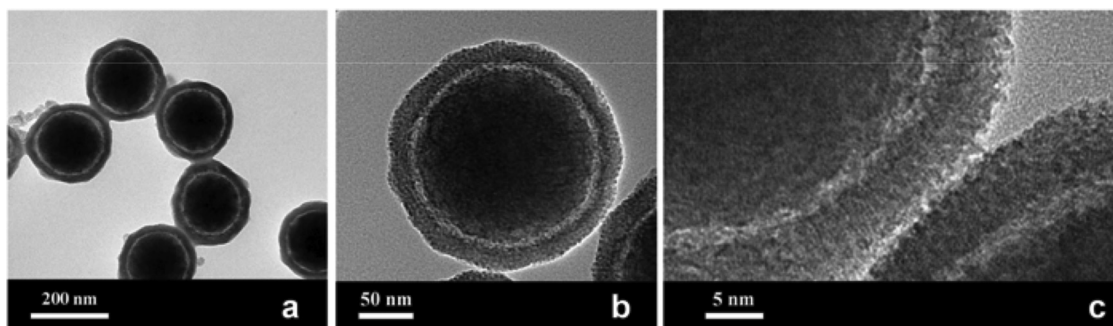
Figure 1. TEM images of the yolk–shell hybrid materials with a PMO shell (YS-PMO-1) at different magnifications. (Scale bars are 200 nm, 50 nm, and 5 nm for (a), (b), (c), respectively).

A high-resolution transmission electron microscopy (HRTEM) image of YS-PMO-1, as shown in Figure 1c, further confirms the ordered organisation of the mesopores in the shell, with a pore size of ~3 nm. As illustrated in **Figure 2**a, low-angle XRD pattern of YS-PMO-1 shows one strong peak in the 2θ range 2°–3°, confirming the mesoscopic ordering in the shell. In contrast to standard MCM41-type silica materials, the PMO shell seems less ordered. Further evidence of the mesoporous structure of YS-PMO-1 could be obtained by N_2 sorption analysis. The adsorption–desorption isotherm obtained on YS-PMO-1 shows a type IV behaviour with a two-step capillary condensation in the relative pressure ranges of 0.1–0.3 and 0.7–0.9 (see Figure 2b), in agreement with the presence of a hierarchical porosity organisation consistent with the yolk–shell structure. The corresponding Barrett–Joyner-Halenda (BJH) pore size distribution shows two peaks, centred at 3 nm and 16 nm, corresponding to the mesopores of the shell and the void between the solid core and the shell, respectively (see Figure 2c). In addition, the Brunauer–Emmett–Teller (BET) specific surface area and total pore volume of YS-PMO-1 are calculated to be 147 m²·g⁻¹ and 0.32 cm³·g⁻¹, respectively (**Table 1**).

For application of yolk–shell nanoparticles in catalysis and drug delivery, a control of the shell thickness is desirable. Previously, we demonstrated the feasibility of the preparation of similar YSNs with different silica shell thickness by controlling

the amount of the silica precursor, namely tetraethyl orthosilicate (TEOS) in that particular case. In the present work, YS-PMO samples with varied shell thickness and void space, designated as YS-PMO-2, YS-PMO-3, and YS-PMO-4, were obtained similarly by tuning the concentration of the BTME precursor, under otherwise similar experimental conditions to those implemented for YS-PMO-1. As shown in **Figure 3**, with increasing of the amount of BTME from 0.17 to 0.32 mL, the shell thickness gradually increased from 16 to 28 nm, and the void space gradually decreased from 18 to 4 nm, respectively, while the mesopores size in the shell remained fairly constant at 2~3 nm (Table 1). However, at very high BTME concentration (0.32 mL), the presence of PMO nanoparticles coexisting with YS-PMO-4 yolk–shell particles was observed. Furthermore, with increasing the amount of BTME added to the synthesis mixture, it was observed that BET surface area and total pore volume of the resulting nanoparticles decreased gradually from 262 to 82 m²·g⁻¹, and 0.46 to 0.18 cm³·g⁻¹, respectively (Table 1 and Figure S1 in the Supporting Information). Investigation of all these samples using SEM indicated that their average diameters agreed fairly well with the sizes observed by the TEM images (i.e., ~220 nm) (Figure S2).

The formation of such a yolk–shell structure is probably a cooperative process of vesicle templating formed by FC4, associated with ripening and shrinkage of the PMO shell. The
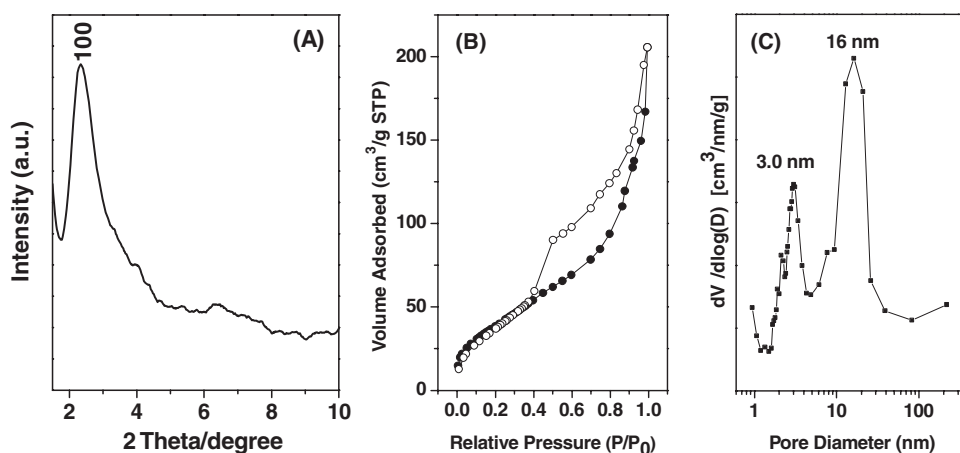

Figure 2. Low-angle XRD pattern (A), nitrogen adsorption-desorption isotherm (B) and respective pore size distribution obtained from the BJH model applied to the adsorption branch (C) of the yolk–shell hybrid with PMO shell (YS-PMO-1).

Table 1. Physicochemical parameters of the different yolk–shell structures.

Sample	BTME amount [mL]	Ethanol amount [mL]	Void space [nm]	Shell thickness [nm]	BET surface area [m² g⁻¹]	Shell pore diameter [nm]ᵃ⁾	Total pore volume [cm³ g⁻¹]
YS-PMO-1	0.22	0	7	20	147	3.0	0.32
YS-PMO-2	0.17	0	18	16	262	2.3	0.46
YS-PMO-3	0.27	0	6	24	127	2.3	0.28
YS-PMO-4	0.32	0	4	28	82	2.3	0.18
YS-PMO-5	0.22	5	20	24	200	2.5	0.26
YS-PMO-6	0.22	10	33	34	228	2.5	0.31
YS-PMO-7	0.22	15	45	34	165	2.5	0.22
YS-PMO-8	0.22	20	52	34	151	2.5	0.24

ᵃ⁾The pore size were calculated by BJH method which was probably underestimated according to previous report.[39]

addition of alcohol is believed to play an essential role in the formation of the vesicles, as it is generally the case.[17,18] To further substantiate the influence of the different synthesis parameter, we studied the role of ethanol present in the synthesis medium on the formation of the yolk–shell PMO materials. As presented in **Figures 4** and S3, under similar conditions as for YS-PMO-1 with a fixed BTME amount of 0.22 mL, the addition of different amounts of ethanol led to the formation of very uniform and well-dispersed hybrid YS-PMO exhibiting different void space. By increasing the volume of ethanol from 5 to 20 mL, the void space increased from 20 to 52 nm (see also Table 1). Here, larger vesicles may form with increasing volume of ethanol added. Surprisingly, the silica core also becomes less regular, from dense to porous, and its size was reduced with increasing the amount of ethanol. To explain this, one can suggest that the core silica spheres are presumably less dense under these conditions being built of networks of disordered and discontinuous interconnection of Si–O–Si and Si–OH bonds. Such silica spheres prepared by the Stober process are formed through aggregation of small nucleus particles, followed by growth via monomer addition. In the presence of a large amount of ethanol, sequences of Si–O–Si and Si–O–C_2H_5 bond-breaking and bond-forming processes in the presence of hydroxide ions could alter the nature of the core, yielding a more porous structure in the presence of BTME. A similar phenomenon was also described by Yang et al.[25] who synthesised yolk–shell hybrids starting from

core–shell nanoparticles by using organosilane as an additive. However, when ethanol (5~20 mL) was used, the pore structure of the PMO shell was less ordered (Figure 4). The reason for the reduced order may be attributed to the increasing critical micelle concentration (CMC) of CTAB in the presence of ethanol. At high concentrations of ethanol, CTAB can interact more strongly with ethanol than with water, which will eventually raise the critical micelle concentration value and thus alter the formation of micelle. These effects are also in an agreement with previous reports,[40–42] which have shown mesophase regression when the ethanol-to-surfactant ratio exceeded 73.8. The lower order of the mesoporous shell of these samples was also judged from low angle XRD (**Figure 5**a) indicative of more distorted 2D hexagonal structures with one broad and weak (100) diffraction peak. Furthermore, the nitrogen sorption analysis results, depicted in Figure 5b, show a type IV isotherm with H2/H4 hybrid hysteresis loop typical of hollow structures with mesoporous wall.[32–35] The mixed H2/H4 loops observed for all samples with parallel and almost horizontal branches at a relative pressure close to the saturation vapour pressure may thus be attributed to the hollow voids between the core and shell. The capillary condensation steps of the isotherms appearing in the relative pressure interval $P/P_0 = 0.25$–0.35 indicate that these materials remained somewhat mesostructured. The pore-size distributions calculated by the BJH method using adsorption branch are shown in Figure 5c for the samples synthesised with
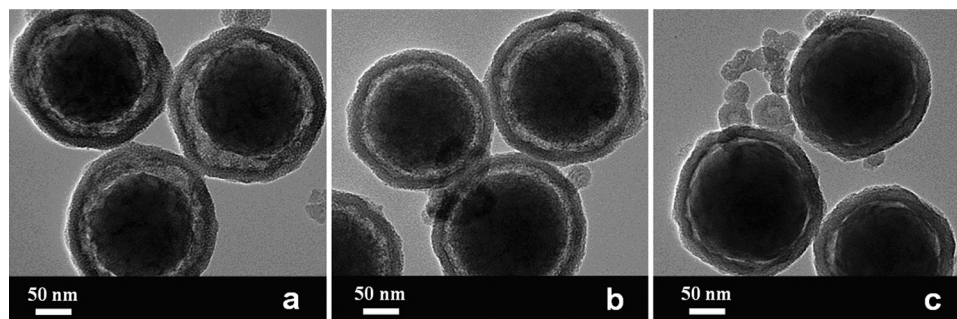

Figure 3. Representative TEM images of the yolk–shell hybrid materials with different thicknesses of PMO shell synthesised at different BTME molar amounts: a) YS-PMO-2, BTME = 0.17 mL; b) YS-PMO-3, BTME = 0.27 mL; c) YS-PMO-4, BTME = 0.32 mL.
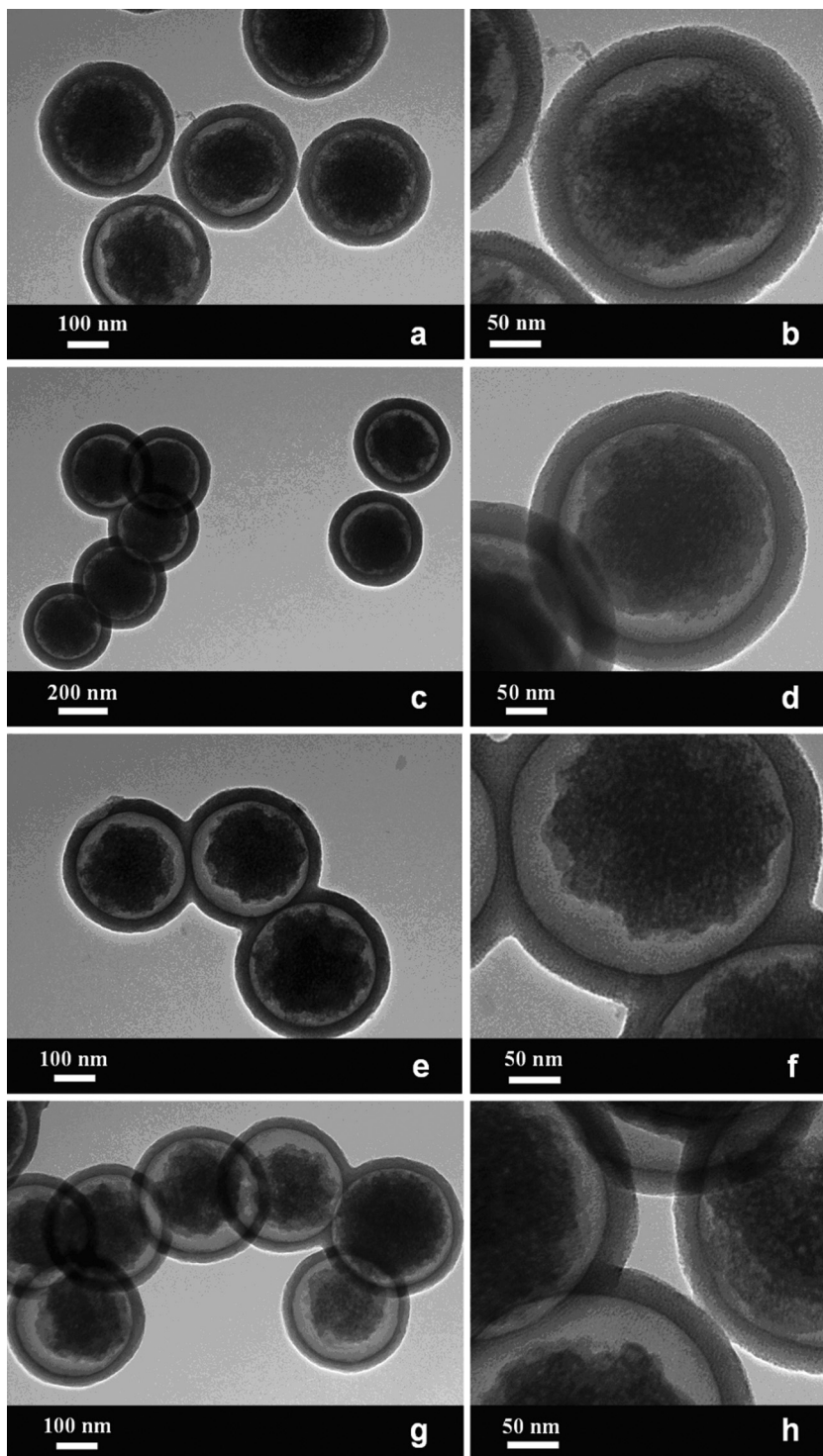
Materials
Views

www.MaterialsViews.com

ADVANCED
FUNCTIONAL
MATERIALS
www.afm-journal.de

FULL PAPER

Figure 4. TEM images of the yolk–shell hybrid materials with PMO shells synthesised with different volumes of ethanol: a,b) 5 mL; c,d) 10 mL; e,f) 15 mL; g,h) 20 mL.

2.2. Characterisation of the Chemical Composition of Yolk–Shell Hybrid Materials with PMO Shell

The chemical composition of YS-PMO was characterised by Fourier-transform infrared (FT-IR) spectroscopy (Figure S4). The C–H vibrations of $-CH_2CH_2-$ appearing in the range 2918–2875 cm^{-1} and at 1160 cm^{-1} are clearly observed in the FT-IR spectra of YS-PMO. The FT-IR spectra of these samples show the Si–C stretching modes at 696 and 768 cm^{-1}, proving the integrity of the ethane organic groups in YS-PMO. Solid-state NMR spectroscopy was performed to further verify the composition of YS-PMO. The resonance at 4.4 ppm in the ^{13}C CP NMR spectrum of YS-PMO can be assigned to the C species of the ethane moiety (**Figure 6**a). The signals at 58.5, 29.8, and 17.3 ppm [labelled with an asterisk (*)] are due to the surfactant residues and the carbons of the ethoxy groups formed during the surfactant extraction process.[32,33,43] The result of solid-state ^{13}C CP MAS NMR confirms the incorporation and integrity of the ethylene organic groups in the YSNs. ^{29}Si NMR spectra of YS-PMO show the existence of both Q^n and T^n sites as expected (Figure 6b). The characteristic resonances in the range of –90 to –110 ppm can be assigned to $(HO)_2Si(OSi)_2$ (Q^2 δ -91), $(HO)Si(OSi)_3$ (Q^3 δ -102), and $Si(OSi)_4$ (Q^4 δ -109) silicon species. These Q species originate from the pure silica core. The sharp signal at –67.6 ppm is attributed to Si atoms bridged by the ethane groups [T^3, $SiC(OSi)_3$]. The T/(T + Q) ratio calculated from the normalized peak areas is 0.40, which corresponds to the estimated shell/core ratio, which is in line with the amount of BTME incorporated. The combined results of NMR and FT-IR analysis establish that the framework of YS-PMO is built of $O_{1.5}Si$-CH_2CH_2-$SiO_{1.5}$ units.

2.3. Encapsulation of Metal Nanoparticles (Au, Pt, Pd) into the PMO-based Yolk–Shell Hybrid Materials

In the following, we will demonstrate the successful incorporation of Au, Pt, and Pd nanoparticles into the structure of YS-PMO-6 acting as a nanoreactor. The synthetic pathway for preparing metal nanoparticles encapsulated into yolk–shell PMO nanoparticles is shown in Scheme 1. After immersion of YS-PMO-6 in an aqueous solution of the given metal salt, the resulting composite was reduced by trisodium citrate to generate metal-loaded yolk–shell nanoparticles (denoted as metal–YS-PMO).

addition of different volumes of ethanol. The physicochemical properties of these samples are listed in Table 1. From these data, it can be seen that all samples possess uniform pore size around 3 nm, high surface areas (151~228 $m^2\ g^{-1}$) and pore volume (0.22~0.31 $cm^3\ g^{-1}$).
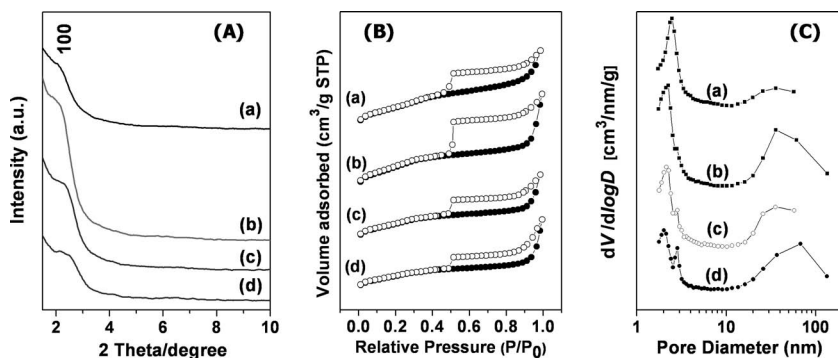
FULL PAPER

Figure 5. Low-angle XRD patterns (A), nitrogen adsorption-desorption isotherms (B), and pore size distributions obtained from the BJH model applied to the adsorption branch (C) of the yolk–shell hybrid materials with PMO shells synthesised with different volumes of ethanol: a) 5 mL; b) 10 mL; c) 15 mL; d) 20 mL.

From the TEM images taken on the metal-loaded yolk–shell PMO samples (**Figure 7** and S5), it can be seen that the metal nanoparticles are mostly located inside the yolk–shell colloidal particles. Furthermore, the monodispersity and yolk–shell architecture of the particles were not affected through the encapsulation of the Au, Pd, and Pt nanoparticles. To directly image the metal nanoparticles in the yolk–shell structures, high-angular annular dark-field scanning transmission electron microscopy (HAADF-STEM) was performed. The HAADF-STEM images (Figure 7c,f,i) provide a clear contrast of the core, the metal nanoparticles, the hollow part and the porous shell. The metal nanoparticles are visualised as bright spherical dots, evidence of the incorporation of particles in the yolk–shell matrix. Energy-dispersive X-ray (EDX) analyses confirmed the presence of Au, Pt, Pd in the yolk–shell particles (Figure S6).

For Au–YS-PMO, two types of Au nanoparticles are visible, coexisting inside the yolk–shell structure. One of the types of Au nanoparticles exhibits a very narrow size distribution, with an average size of about 2 nm, as estimated from the TEM and HAADF-STEM images. The second type of Au nanoparticles which have a size around 20 nm is probably formed by sintering of adjacent small Au nanoparticles during synthesis. The size of the incorporated Au nanoparticle can be controlled by tuning the initial concentration of $HAuCl_4$. At mean time,

the weight fraction of these metal nanoparticles was increased with the increase of the concentration of $HAuCl_4$. In the case of Pt-YS-PMO, it is evident from the TEM and HAADF-STEM images that Pt nanoparticles with 3 nm coexist together with aggregates of Pt nanoparticles exhibiting a more or less dendritic shape. Finally, for the Pd-YS-PMO, similarly to Au and Pt, small palladium particles (~3 nm) together with larger aggregated particles can be observed (Figure 7g–i). These results are consistent with the well-documented aggregation of noble metal nanoparticles through Ostwald ripening and formation of metal–Cl complex nanostructures in silica shells as previously exploited by Lou et al.[14] In this previous work, gold nanoparticles with different morphologies including triangular and rodlike shapes were formed through Ostwald ripening in multicore Au–silica hollow particles.

2.4. Selective Oxidation Reactions using Pd–YS-PMO as a Catalytic Nanoreactor

The selective oxidation of alcohols to aldehydes remains an important task in many important industrial and fine chemicals production processes. Of particular current interest is the use of molecular oxygen as the oxidant because it represents a green chemical process, in contrast to the use of toxic and expensive stochiometric oxidants based on metal oxides. Thus, the selective oxidation profiles of a wide range of primary and secondary alcohols were thus studied over Pd–YS-PMO catalysts (Pd loading of 5 mol%), in the presence of O_2. For benzyl alcohol and methyl-substituted benzylic alcohol, conversions of 94% and 92% were obtained within 8 h, respectively (**Table 2**, entries 1 and 2). The selectivity for the target products was evaluated to be higher than 99%. In the case of CH_3O-substituted benzylic alcohol, a total conversion with selectivity > 99% was also achieved over 8 h under O_2 atmosphere (Table 2, entry 3). Similarly, cinnamyl alcohol was totally converted to cinnamaldehyde under the same conditions. The selectivity for
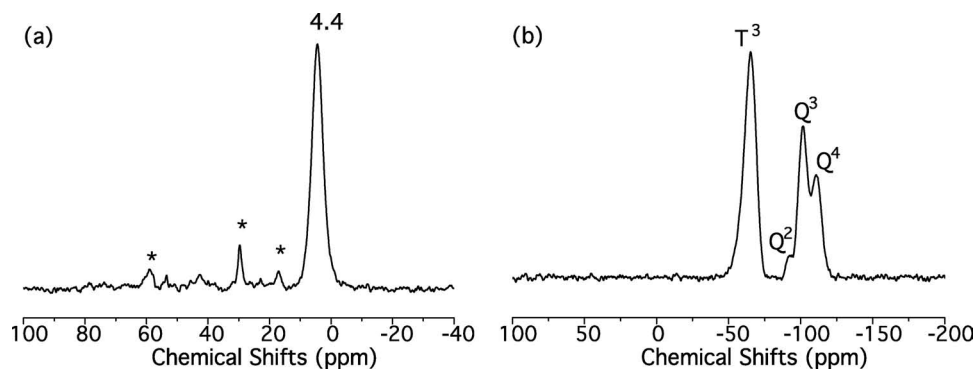

Figure 6. Solid-state ^{13}C CP MAS NMR spectra (a) and ^{29}Si NMR spectra (b) of YS-PMO-1.

Materials Views
www.MaterialsViews.com

ADVANCED
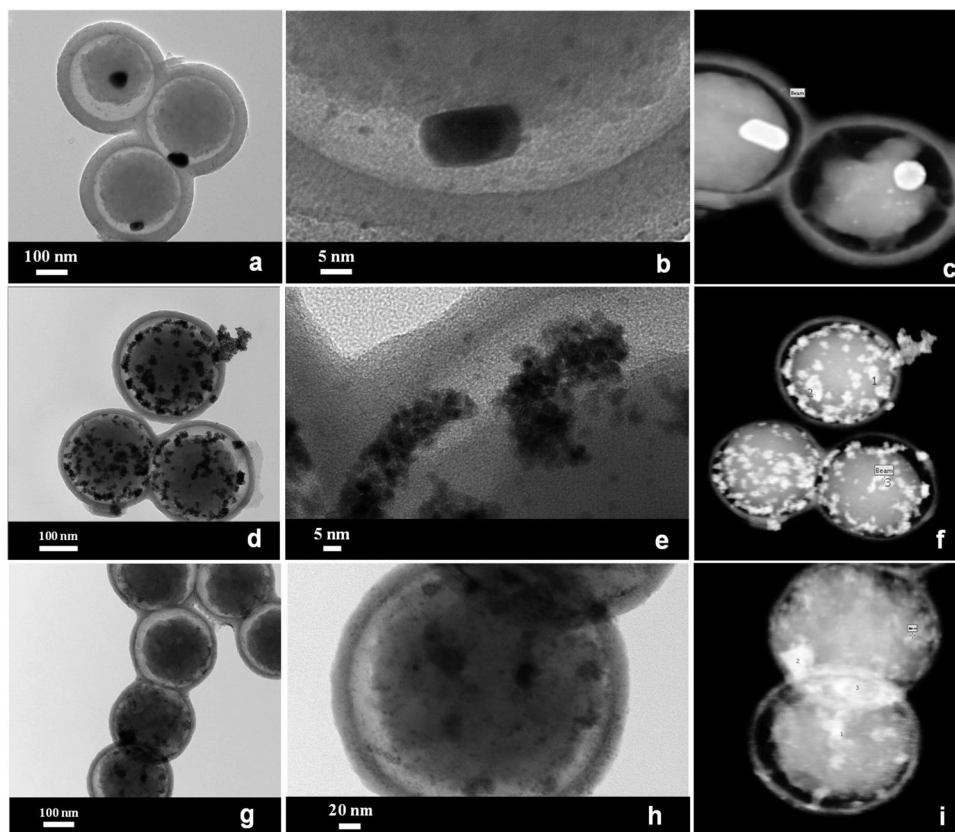FUNCTIONAL
MATERIALS
www.afm-journal.de

FULL PAPER

Figure 7. a),d,g,) TEM images, b,e,h,) HRTEM images, and c,f,i) HAADF-STEM images of Au–YS-PMO (a–c); Pt–YS-PMO (d–f); Pd–YS-PMO (g–i).

α,β-unsaturated aldehyde was again superior to 99% (Table 2, entry 4). In the case of 3-methyl-2-butanol, as an example of typical aliphatic alcohol, the catalyst Pd–YS-PMO showed a moderate activity with, nevertheless, an excellent selectivity (Table 2, entry 5). As such, under the conditions used, the selectivity to the corresponding aldehyde is in all cases superior to 99%.

No detectable carboxylic acid species were found among the products, confirming the high selectivity to the aldehyde. The excellent catalytic activity toward various oxygenate substrates demonstrates that the mesoporous shell around the encapsulated metal catalyst allows the reaction molecules to freely access to the encapsulated metal sites. Moreover, the protective

Table 2. Selective oxidation of various alcohols into aldehyde over Pd-YS-PMO nanoreactors.

Entry[a]	Substrates	Products	RT[b] [°C]	Time [h]	Conversion [%]	Selectivity[c] [%]
1	(benzyl alcohol) —CH$_2$OH	(benzaldehyde) —CH$_2$	50	8	94	>99
2	—⟨⟩—CH$_2$OH	—⟨⟩—CHO	50	8	92	>99
3	H$_3$CO—⟨⟩—CH$_2$OH	H$_3$CO—⟨⟩—CHO	50	8	100	>99
4	(cinnamyl alcohol) —OH	—CHO	50	8	100	>99
5	—OH	—CHO	50	8	53	>99

[a]The reaction was carried out in O$_2$ atmosphere in the presence of 5 mol% Pd with water as solvent; [b]RT: reaction temperature; [c]Selectivity to aldehyde.

**ADVANCED
FUNCTIONAL
MATERIALS**

www.afm-journal.de

Materials Views

www.MaterialsViews.com

FULL PAPER

mesoporous shells could prevent sintering of the metal nano-particles.[44–46] With almost identical Pd loading, Pd–YS-PMO exhibits better catalytic behaviors than that of conventional Pd/SiO₂ and Pd/C.[47] This can be attributed to the yolk shell structures of support. In our system, the metal Pd nanoparticles are thus stabilised while being freely accessible in the void between the core and shell, which seems to be a substantial advantage for exposing all of the active surfaces more efficiently. The high activity of the catalyst suggests that the hollow space in the yolk–shell catalysts could be beneficial for enhanced adsorption of the organic reactant molecules.

3. Conclusions

In conclusion, we have demonstrated that it is possible to fabricate various yolk–shell nanostructures possessing well-defined functional mesoporous inorganic–organic hybrid shells, with tailored shell thickness and void space, using a simple soft templating method. Moreover, our contribution shows that Au, Pt, and Pd nanoparticles can easily be encapsulated into the yolk–shell PMO structure by the impregnation and reduction of adequate metal precursors. This, in turn, enables the creation of highly efficient nanoreactors for catalytic conversions. For instance, the high conversion (~100%) and selectivity (~99%) observed in the case of selective alcohol oxidation reactions performed over Pd-loaded yolk–shell materials tend to confirm that these Pd–YS-PMO could be promising catalysts for fine chemical production. Here, it is clear that the presence of the hollow space in the YSNs played a crucial role in promoting activity and enhancing stability of the metal nanoparticles. Moreover, it is expected that such metal nanoparticle yolk–shell nanoreactors will serve as a useful platform to study reactivity in heterogeneous catalysis as the diffusion of reactants and morphology of active catalysts can readily be manipulated through rational catalyst design. The synthesis strategy reported in this paper may open up new opportunities for preparing yolk shell structured nanomaterials with various compositions. Alternatively, other promising prospects of applications of these materials will be as nanocarriers for controlled delivery and release of therapeutic and bioactive agents; the hierarchical organisation of the pores enabling here co-delivery of multiple agents and multi-step release processes.

4. Experimental Section

Chemicals: All materials were analytical grade and used as received without any further purification. CTAB, BTME (96%), TEOS (>99%), gold chloride (HAuCl₄·3H₂O), H₂PtCl₆·6H₂O (99.95%), Pd(NO₃)₂·xH₂O, were purchased from Aldrich. Fluorocarbon surfactant, FC4, was bought from Yick Vic Chemicals (Hong Kong). Water was purified by a Milli Q system and had an electrical resistance of 18 MΩ·cm.

Synthesis of Monodisperse Silica Spheres: Monodisperse silica spheres (160 nm) were synthesised by mixing 5.5 mL of aqueous ammonia (NH₄OH, 28 wt%) with a solution containing 250 mL of absolute ethanol (EtOH) and 20 mL of deionised water (H₂O). After stirring for 1 h, 15 mL of TEOS was added to the solution and stirred for 6 h at room temperature.[17]

Synthesis of Yolk–Shell Hybrid Materials with Mesoporous Silica Core and PMO Shell: In a typical procedure, 0.15 g of FC4 was dissolved in 30 mL of water and stirred at room temperature for 1 h to prepare the solution

A, solution **B** was prepared by dissolving 0.54 g of the core materials in 18 mL water (30 mg mL⁻¹) and subject to ultrasonic treatment for 30 min. After that, solution **B** was added into solution **A** and stirred for 2 h, before the addition of 0.15 g of CTAB and 0.35 mL of 2 M NaOH. Then, the system was kept at a constant temperature of 80 °C, and 0.17 mL of BTME was introduced at once under vigorous stirring for 24 h. After cooling down to room temperature, the white precipitates were collected by centrifugation and dried at room temperature. Finally, the surfactant CTAB and FC4 was extracted by refluxing 1.0 g of the as-synthesised material in 200 mL of ethanol containing 1.5 g of concentrated HCl aqueous solution for 24 h. The resulting powder products were denoted as YS-PMO-n.

Encapsulation of Metal Nanoparticles (Au, Pt, Pd) into the YS-PMO Materials: Typically, 0.4 g of extracted YS-PMO-6 were impregnated with an aqueous solution of the selected metal salts (14 mL). The concentration of HAuCl₄, H₂PtCl₆, or Pd(NO)₃ was 0.05 M. After sonication for 30 min in an ultrasonic bath, the particles were heated in an oven at 100 °C for 6 h. The dried particles were washed with water for several times, which was to ensure the removal of the nanoparticle outside of YSNs. Finally, the resulting particles were collected by centrifugation and dried for 4 h in a vacuum oven at ambient temperature.

Characterisation: XRD measurements were performed on a Rigaku D/max-2550V diffractometer using Co K$_\alpha$ radiation at 30 kV and 15 mA. SEM images of the samples coated with platinum were recorded on a JEOL 6300 microscope operated at 5–10 kV. TEM images and HAADF-STEM images were obtained by JEOL JEM 2100 and FEI Tecnai F20 electron microscope with an acceleration voltage 200 kV. The powder samples for the TEM measurements were suspended in ethanol and then dropped onto the Cu grids with holey carbon films. Nitrogen sorption isotherms of samples were obtained with a Quantachrome Autosorb-1 and a Quadrasorb SI analyzer at –196 °C. Prior to the measurement, the samples were out-gassed at 120 °C for 12 h. BET specific surface areas were calculated using adsorption data in a relative pressure range of P/P_0 = 0.05~0.25. Pore size distributions were derived from the adsorption branch using BJH method. The total pore volumes were estimated from the amounts adsorbed at a relative pressure (P/P_0) of 0.99. Solid-state ¹³C (100.5 MHz) cross-polarisation magic angle spinning (CP-MAS) and ²⁹Si (79.4 MHz) MAS NMR experiments were recorded on a Bruker MSL-300 spectrometer. The spectrometer was equipped with a 4-mm double air bearing, magic angle spinning probe for MAS experiments. The proton 90° pulse time used in the CP-MAS method was 5.5 µs, the acquisition time was 45 ms, cross-polarisation time 2 ms and the relaxation delay was 3 s. The spectrum width was 50 kHz, and 4000 data points were collected over 2000 scans. The experimental parameters were 8 kHz spin rate, 1ms contact time, repetition delay 3s, 20K scans collected for ¹³C CP NMR experiments and 8 kHz spin rate, 5 ms contact time, repetition delay 3 s, 20 K scans for ²⁹Si MAS NMR experiments. FT-IR spectra were collected with a Nicolet Nexus 470 IR spectrometer with KBr pallet.

Catalytic Reaction: The given alcohol (1 mmol), water (2 mL) and the Pd–YS-PMO catalyst were combined in a dry flask, and the mixture was stirred at given temperature in O₂ for a given time. Oxygen gas was introduced into the flask from an O₂ balloon under atmospheric pressure. After the reaction, the liquid was extracted with diethyl ether. The resulting organic layer was dried with Na₂SO₄ and then analysed with GC to determine the conversion and selectivity.

Supporting Information

Supporting Information is available from the Wiley Online Library or from the author.

Acknowledgements

FULL PAPER

[1] J. Liu, S. Z. Qiao, J. S. Chen, X. W. Lou, X. R. Xing, G. Q. Lu, *Chem. Commun.* **2011**, *47*, in press, DOI:10.1039/c1cc13658e.
[2] Y. D. Yin, R. M. Rioux, C. K. Erdonmez, S. Hughes, G. A. Somorijai, A. P. Alivisatos, *Science* **2004**, *304*, 711.
[3] Y. Zhao, L. Jiang, *Adv. Mater.* **2009**, *21*, 3621.
[4] X. W. Lou, L. A. Archer, Z. Yang, *Adv. Mater.* **2008**, *20*, 3987.
[5] K. Kamata, Y. Lu, Y. N. Xia, *J. Am. Chem. Soc.* **2003**, *125*, 2384.
[6] J. Lee, J. C. Park, H. Song, *Adv. Mater.* **2008**, *20*, 1523.
[7] Y. Chen, H. R. Chen, M. Ma, F. Chen, L. M. Guo, L. X. Zhang, J. L. Shi, *J. Mater. Chem.* **2011**, *21*, 5290.
[8] L. Zhang, S. Z. Qiao, Y. G. Jin, Z. G. Chen, H. C. Gu, G. Q. Lu, *Adv. Mater.* **2008**, *20*, 805.
[9] M. Roca, A. J. Haes, *J. Am. Chem. Soc.* **2008**, *130*, 14273.
[10] G. Chen, Y. Wang, M. X. Yang, J. Xu, S. J. Goh, M. Pan, H. Y. Chen, *J. Am. Chem. Soc.* **2010**, *132*, 3644.
[11] J. Liu, H. Xia, D. F. Xue, L. Lu, *J. Am. Chem. Soc.* **2009**, *131*, 12086.
[12] X. W. Lou, C. Yuan, L. A. Archer, *Adv. Mater.* **2007**, *19*, 3328.
[13] W. M. Zhang, J. S. Hu, Y. G. Guo, S. F. Zheng, L. S. Zhong, W. G. Song, L. J. Wan, *Adv. Mater.* **2008**, *20*, 1160.
[14] X. W. Lou, C. Yuan, E. Rhoades, Q. Zhang, L. A. Archer, *Adv. Funct. Mater.* **2006**, *16*, 1679.
[15] X. J. Wu, D. S. Xu, *J. Am. Chem. Soc.* **2009**, *131*, 2774.
[16] X. J. Wu, D. S. Xu, *Adv. Mater.* **2010**, *22*, 1516.
[17] J. Liu, S. Z. Qiao, S. B. Hartono, G. Q. M. Lu, *Angew. Chem. Int. Ed.*, **2010**, *49*, 4981.
[18] J. Liu, R. Harrison, J. Z. Zhou, T. T. Liu, C. Z. Yu, G. Q. M. Lu, S. Z. Qiao, Z. P. Xu, *J. Mater. Chem.* **2011**, *21*, 10641.
[19] T. R. Zhang, J. P. Ge, Y. X. Hu, Q. Zhang, S. Aloni, Y. D. Yin, *Angew. Chem. Int. Ed.* **2008**, *47*, 5806.
[20] Q. Zhang, J. P. Ge, J. Goebl, Y. X. Hu, Z. D. Lu, Y. D. Yin, *Nano Res.* **2009**, *2*, 583.
[21] D. Chen, L. L. Li, F. Q. Tang, S. Qi, *Adv. Mater.* **2009**, *21*, 3804.
[22] L. F. Tan, D. Chen, H. Y. Liu, F. Q. Tang, *Adv. Mater.* **2010**, *22*, 4885.
[23] Y. F. Zhu, E. Kockrick, T. Ikoma, N. Hanagata, S. Kaskel, *Chem. Mater.* **2009**, *21*, 2547.
[24] Y. J. Wong, L. F. Zhu, W. S. Teo, Y. W. Tan, Y. H. Yang, C. Wang, H. Y. Chen, *J. Am. Chem. Soc.* **2011**, *133*, 9510.
[25] Y. Yang, J. Liu, X. B. Li, X. Liu, Q. H. Yang, *Chem. Mater.* **2011**, *23*, 3676.
[26] B. Liu, H. C. Zeng, *Small* **2005**, *1*, 566.
[27] E. C. Cho, P. H. C. Camargo, Y. N. Xia, *Adv. Mater.* **2010**, *22*, 744.
[28] A. Sayari, S. Hamoudi, Y. Yang, I. L. Moudrakovsk, J. R. Ripmeester, *Chem. Mater.* **2000**, *12*, 3857.
[29] Q. H. Yang, J. Liu, L. Zhang, C. Li, *J. Mater. Chem.* **2009**, *19*, 1945.
[30] F. Hoffmann, M. Cornelius, J. Morell, M. Fröba, *Angew. Chem. Int. Ed.* **2006**, *45*, 3216.
[31] V. Rebbin, R. Schmidt, M. Fröba, *Angew. Chem., Int. Ed.* **2006**, *45*, 5210.
[32] J. Liu, S. Bai, H. Zhong, C. Li, Q. H. Yang, *J. Phys. Chem. C* **2010**, *114*, 953.
[33] J. Liu, Q. H. Yang, L. Zhang, H. Q. Yang, J. S. Gao, C. Li, *Chem. Mater.* **2008**, *20*, 4268.
[34] H. Djojoputro, X. F. Zhou, S. Z. Qiao, L. Z. Wang, C. Z. Yu, G. Q. Lu, *J. Am. Chem. Soc.* **2006**, *128*, 6320.
[35] S. Z. Qiao, C. X. Lin, Y. G. Jin, Z. Li, Z. M. Yan, Z. P. Hao, Y. N. Huang, G. Q. Lu, *J. Phys. Chem. C* **2009**, *113*, 8673.
[36] S. Guan, S. Inagaki, T. Ohsuna, O. Terasaki, *J. Am. Chem. Soc.* **2000**, *122*, 5660.
[37] X. J. Meng, T. Yokoi, D. L. Lu, T. Tatsumi, *Angew. Chem. Int. Ed.* **2007**, *46*, 7796.
[38] S. Haffer, M. Tiemann, M. Froba, *Chem. Eur. J.* **2010**, *16*, 10447.
[39] M. Jaroniec, L. A. Solovyov, *Chem. Commun.* **2006**, 2242.
[40] D. C. Niu, Z. Ma, Y. S. Li, J. L. Shi, *J. Am. Chem. Soc.* **2010**, *132*, 15144.
[41] A. M. El-Toni, M. W. Khan, M. A. Ibrahim, M. Abid, M. Al-Hoshana, M. Al-salhia, *Chem. Commun.* **2010**, *46*, 6482.
[42] W. Q. Wang, J. G. Wang, P. C. Sun, D. T. Ding, T. H. Chen, *J. Colloid Interface Sci.* **2009**, *331*, 156.
[43] W. P. Guo, F. Kleitz, K. H. Cho, R. Ryoo, *J. Mater. Chem.*, **2010**, *20*, 8257.
[44] J. Liu, S. Z. Qiao, Q. H. Hu, G. Q. Lu, *Small*, **2011**, *7*, 425.
[45] Y. H. Deng, Y. Cai, Z. K. Sun, J. Liu, C. Liu, J. Wei, W. Li, C. Liu, Y. Wang, D. Y. Zhao, *J. Am. Chem. Soc.* **2010**, *132*, 8466.
[46] P. M. Arnal, M. Comotti, F. Schüth, *Angew. Chem. Int. Ed.* **2006**, *45*, 8224.
[47] M. Besson, P. Gallezot, *Catal. Today* **2000**, *57*, 127.